Hyperaccumulator *Alyssum murale* relies on a different metal storage mechanism for cobalt than for nickel

R. Tappero[1], E. Peltier[1], M. Gräfe[1], K. Heidel[1], M. Ginder-Vogel[2], K. J. T. Livi[3], M. L. Rivers[4], M. A. Marcus[5], R. L. Chaney[6] and D. L. Sparks[1]

[1]Plant and Soil Sciences, University of Delaware, Newark, DE 19716, USA; [2]Geological and Environmental Sciences, Stanford University, Stanford, CA 94305, USA; [3]Earth and Planetary Sciences, John Hopkins University, Baltimore, MD 21218, USA; [4]Geophysical Sciences and Center for Advanced Radiation Sources, University of Chicago, Chicago, IL 60637, USA; [5]Advanced Light Source, Lawrence Berkeley National Laboratory, Berkeley, CA 94720, USA; [6]USDA-ARS, Environmental Management and By-products Utilization, Beltsville, MD 20705, USA

Author for correspondence:
R. Tappero
Tel: +1 302 831 1230
Fax: +1 302 831 0605
Email: rtappero@udel.edu

Received: *31 January 2007*
Accepted: *23 April 2007*

Summary

- The nickel (Ni) hyperaccumulator *Alyssum murale* has been developed as a commercial crop for phytoremediation/phytomining Ni from metal-enriched soils. Here, metal co-tolerance, accumulation and localization were investigated for *A. murale* exposed to metal co-contaminants.
- *A. murale* was irrigated with Ni-enriched nutrient solutions containing basal or elevated concentrations of cobalt (Co) or zinc (Zn). Metal localization and elemental associations were investigated *in situ* with synchrotron X-ray microfluorescence (SXRF) and computed-microtomography (CMT).
- *A. murale* hyperaccumulated Ni and Co (> 1000 μg g^{-1} dry weight) from mixed-metal systems. Zinc was not hyperaccumulated. Elevated Co or Zn concentrations did not alter Ni accumulation or localization. SXRF images showed uniform Ni distribution in leaves and preferential localization of Co near leaf tips/margins. CMT images revealed that leaf epidermal tissue was enriched with Ni but devoid of Co, that Co was localized in the apoplasm of leaf ground tissue and that Co was sequestered on leaf surfaces near the tips/margins.
- Cobalt-rich mineral precipitate(s) form on leaves of Co-treated *A. murale*. Specialized biochemical processes linked with Ni (hyper)tolerance in *A. murale* do not confer (hyper)tolerance to Co. *A. murale* relies on a different metal storage mechanism for Co (exocellular sequestration) than for Ni (vacuolar sequestration).

Key words: *Alyssum murale*, cobalt (Co), computed-microtomography (CMT), hyperaccumulation, nickel (Ni), synchrotron X-ray microfluorescence (SXRF), tolerance.

New Phytologist (2007) **doi**: 10.1111/j.1469-8137.2007.02134.x

Introduction

Large-scale metal contamination can result in severe environmental damage, and remediation efforts represent a substantial financial burden for industry, government and taxpayers. Anthropogenic metal inputs include spoil from metal mining operations, fallout from refinery emissions, waste disposal, electroplating, combustion of fossil fuels, and agricultural application of pesticides and biosolids (Adriano, 1986). Traditional remediation efforts (e.g. excavation, burial and contaminant isolation) are not feasible for large-scale impacts and therefore alternative remediation strategies are necessary when vast areas of land have been contaminated. Hyperaccumulator plants concentrate trace metals in their harvestable biomass (Brooks *et al.*, 1977), thereby offering a sustainable treatment option for metal-contaminated sites (phytoextraction) and an opportunity to mine metal-rich soils (phytomining) (Chaney, 1983). Cultivating nickel (Ni)

hyperaccumulator plants on metal-enriched soils and ashing the harvestable biomass to produce Ni ore (bio-ore) is an economically viable alternative for metal recovery (Chaney *et al.*, 2004).

Soils suitable for Ni phytomining include serpentine soils and industrially contaminated soils. Serpentine soils develop from ultramafic parent material and thus contain appreciable quantities of Ni, cobalt (Co), chromium (Cr), manganese (Mn), iron (Fe) and zinc (Zn). The Ni : Co ratios in serpentine soils typically range from 5 to 10. Anthropogenic metal inputs generally involve discharge of a mixed-element waste stream. For instance, emissions from Ni smelters are typically enriched with other trace metals from the ore (e.g. copper (Cu), Co, lead (Pb) and Zn). Heavy metals are incorporated into (metallo)enzymes and are thereby toxic to living organisms in excessive amounts. Cobalt contamination is an environmental concern, and the radionuclide ^{60}Co is classified as a priority pollutant (Hamilton, 1994). Hyperaccumulator plants used to extract Ni from metal-enriched soils must be tolerant of co-contaminants. Therefore, the effects of metal co-contaminants on the physiology and biochemistry of hyperaccumulators, and ultimately on the efficiency of metal phytoextraction, is of concern for metal recovery efforts.

Several first-row transition metals (e.g. Co and Ni) have important roles in biological systems as activators of enzymes or as key components of enzyme systems. Cobalt is essential for *Rhizobium* (it associates symbiotically with legume roots for N_2 fixation), free-living nitrogen-fixing bacteria (e.g. *Azotobacter* spp.) and cyanobacteria. However, there is no evidence that Co has a direct role in the metabolism of higher plants (Marschner, 1995). Nickel is the element most recently classified as an 'essential' plant nutrient (Welch, 1995) and is a key component of the Ni-containing enzyme, urease (Dixon *et al.*, 1975). Transmembrane transport systems with specificity for Ni or Co have not been identified in higher plants.

The nickel hyperaccumulator, *Alyssum murale*, a herbaceous perennial (*Brassicaceae* family) native to Mediterranean serpentine soils, has been developed as a commercial crop for phytoremediation/phytomining (Chaney, 1983, 2004; Li *et al.*, 2003a). Hyperaccumulator species of *Alyssum* (hereafter referred to as '*Alyssum*') accumulate Co from Co-enriched soils (Homer *et al.*, 1991; Malik *et al.*, 2000); Cobalt accumulation is most efficient in mildly acidic soils, whereas Ni is most effectively accumulated from neutral soils (Li *et al.*, 2003b; Kukier *et al.*, 2004). *Alyssum* sequesters Ni via epidermal compartmentalization, a metal sequestration strategy exploiting leaf epidermal tissue as the sink for metal storage. Epidermal cell vacuoles are responsible for Ni sequestration in *Alyssum* (Krämer *et al.*, 1997a, 2000; Broadhurst *et al.*, 2004a,b), and vacuolar sequestration has been recognized as a key component of cellular-level metal tolerance (i.e. (hyper)tolerance) for several hyperaccumulator species (Heath *et al.*, 1997; Mesjasz-Przybylowicz *et al.*, 1997; Küpper *et al.*, 1999, 2000, 2001; Frey *et al.*, 2000; Bidwell *et al.*, 2004; Küpper & Kroneck, 2005). However, Co sequestration in *Alyssum* epidermal cell vacuoles has not been reported previously.

Information regarding metal localization (e.g. tissue, cells and organelles) and elemental associations in accumulator plants is crucial to understanding the mechanisms of hyperaccumulation and tolerance. Synchrotron-based techniques such as X-ray microfluorescence (SXRF) and computed-microtomography (CMT) can be used to image (*in situ*) elements in hyperaccumulator plants. SXRF imaging of an intact, transpiring thallium (Tl) accumulator (*Iberis intermedia*) showed that Tl is distributed throughout the vascular network, and X-ray absorption spectroscopy (XAS) identified aqueous Tl (I) as the primary species in plant tissue (Scheckel *et al.*, 2004). X-ray CMT imaging techniques such as differential absorption (DA-CMT) and fluorescence microtomography (F-CMT) resolve the three-dimensional distribution of elements within a sample, and hydrated biological specimens can often be analyzed with minimal or no sample preparation and alteration. DA-CMT and F-CMT were used to visualize Fe localization in seeds of mutant and wild-type *Arabidopsis*, revealing that Fe storage in seeds was mediated by the vacuolar Fe transporter (VIT1) (Kim *et al.*, 2006). F-CMT and DA-CMT showed Ni enrichment in leaf epidermal tissue of *A. murale* grown in Ni-contaminated soils (McNear *et al.*, 2005).

Soils naturally enriched or industrially contaminated with Ni typically have co-contaminants present; however, the influence of common metal co-contaminants on Ni hyperaccumulation remains poorly understood. In the present work, the effect of Co and Zn on Ni accumulation and localization in *A. murale* was examined. Metal localization and elemental associations in plants were investigated with X-ray and electron microscopies and X-ray microtomography. Particular emphasis was placed on the phenomenon of 'simultaneous hyperaccumulation' (Ni and Co) and its relationship to metal co-tolerance.

Materials and Methods

A. murale (Waldst. & Kit.) accession 'Kotodesh' (common name madwort or yellowtuft) was tested for growth and metal uptake in response to elevated Co and Zn concentrations in pseudo-hydroponic culture. Cobalt was selected as a competing divalent metal based on its geogenic association with Ni (co-occurrence in serpentine soils, metal ores and smelter/refinery emissions) and because previous research indicated that *Alyssum* hyperaccumulates Co. Zinc was selected as a divalent metal because it is a common contaminant in surface soils and is not hyperaccumulated by *Alyssum*.

Ebb-and-flow mesocosm design

Each ebb-and-flow mesocosm consisted of two nest-and-stack totes (L.K. Goodwin Co., Providence, RI, USA; models

35180 & 35185), a water pump (Rio® 400; Taam Inc., Camarillo, CA, USA) fitted with 1.27-cm-diameter tubing, and fill/drain and overflow plumbing accessories (American Hydroponics, Arcata, CA, USA). A pump was placed in the reservoir and pump tubing was connected to the plant tray via the fill/drain plumbing accessory. Overflow plumbing consisted of a riser used to maintain the solution level (5 cm) in the plant tray when the pump was running. Ebb-and-flow systems were flooded for 15 min every 8 h, and solution remaining in the tray drained to the reservoir by gravity following each flooding cycle. Mesocoms contained 5–10 l of nutrient solution and six individual plants in 10-cm pots.

Plant propagation

A. murale seeds were germinated in perlite and allowed to develop into mature plants. One mature 'mother' plant was selected for vegetative propagation to minimize variation within the treatment population. Apical cuttings were collected from the 'mother' plant, and leaves or small branches were removed from the lower part of the excised stems. Stems (lower section) were treated with indole-3-butyric acid (rooting hormone) and placed in propagation cubes (Grodan®, Roermond, the Netherlands). *A. murale* cuttings were kept in a clone box (constant light and high humidity) until roots protruded from the cube bottom and were then transferred into pots filled with acid-washed and rinsed perlite. Plastic mesh covered the drainage holes to retain the perlite, and a layer of inert rock was placed on top of the perlite to minimize light penetration and algal growth.

Plant growth conditions

A. murale plants were transferred to a greenhouse and precultured for 3 wk before metal exposure. The photoperiod was set to 16 h with > 400 μmol m^{-2} s^{-1} photosynthetically active radiation from a combination of high-pressure sodium (HPS) lamps and natural sunlight. Temperature was maintained at 25°C and 20°C during the day and night, respectively. Plants were irrigated with nutrient solution designed to mimic serpentine soil conditions (3.1 mM nitrate (NO_3); 0.33 mM phosphate (PO_4); 2.33 mM potassium (K); 1.25 mM magnesium (Mg); 0.5 mM calcium (Ca); 0.25 mM sulfate (SO_4); 10 μM boron (B); 10 μM Mn; 5 μM Zn; 0.1 μM Cu; 0.25 μM molybdenum (Mo); 20 μM Fe-*N,N′*-di-(2-hydroxybenzoyl)-ethylenediamine-*N,N′*-diacetic acid) (Fe(III)-HBED)). Fe(III)-HBED was used to avoid metal–chelator interactions (Chaney, 1988) and to prevent Co(II) oxidation via the formation of amine–Co complexes (Norkus *et al.*, 2001). Nutrient solutions were buffered at pH 6.1 with 2 mM 2-(N-morpholino)-ethane sulfonic acid (MES). Nickel, Co and Zn were added to the nutrient solution from nitrate salt stock solutions to a final concentration of 50 μM. Nutrient solutions contained one of four metal treatments (Ni, Ni+Co, Ni+Zn and Ni+Co+Zn). Treatments were arranged in a randomized complete block statistical design ($n = 5$).

Plant tissue analyses

Plants were harvested after 30 d of metal exposure and analyzed for total metal and nutrient content. Immediately following harvesting, shoots were rinsed in deionized water to remove adhering particles. Roots were meticulously separated from the perlite media and rinsed with 0.001 M $CaCl_2$ followed by deionized water. Plant material was oven-dried at 65°C to a constant weight (approx. 48 h). Dry plant tissue was ground with a plastic herb grinder (420 Grinder, Hempster, London, UK) and homogenized. Plant tissue samples were acid digested using a modified US Environmental Protection Agency (EPA) 3051 method. For each sample, 0.50 g (± 0.05 g) of tissue was microwave digested in 10 ml of concentrated HNO_3. Digests were filtered (0.22 μm) and brought to 30 ml total volume with deionized water. Samples were analyzed by inductively coupled plasma-atomic emission spectrometry (ICP-AES) using yttrium (Y) as an internal standard. Sample duplicates were within 5% agreement, and the Ni, Co and Zn levels measured for the US National Institute of Standards and Technology (NIST) spinach standard (2385) were within the range specified by the NIST. Statistical analyses were performed in MINITAB 12. Analysis of variance (ANOVA) with mean separation by Tukey's HSD ($P < 0.05$) was used to test statistical significance of the treatment effects on yield and elemental composition of plant tissue.

Scanning electron microscopy with energy-dispersive X-ray spectroscopy

A. murale leaves from a Co-treated plant were imaged using scanning electron microscopy (SEM) with energy-dispersive X-ray spectroscopy (EDS), and EDS spectra were collected from the leaf-tip and bulk-leaf regions. Backscattered electron images (BSE) and EDS spectra were recorded using a JEOL 8600 Superprobe (Tokyo, Japan) equipped with an EDAX light-element EDS detector and GENESIS software. The beam energy was set at 20 keV and the beam current at 30 nA (approx. 2 μm spot). Leaves were mounted onto a conductive carbon stub and desiccated ($CaCl_2$) for 48 h before analysis. Samples were sputter-coated with carbon to minimize charging effects.

Synchrotron X-ray microfluorescence and computed-microtomography

Metal localization and elemental associations in *A. murale* plants were investigated with SXRF and CMT. SXRF images were acquired from beamline 10.3.2 of the Advanced Light

Source (ALS) at Lawrence Berkeley National Laboratory (Berkeley, CA, USA) (Marcus *et al.*, 2004). Briefly, this beamline uses Kirkpatrick-Baez (K-B) mirrors to produce a focused spot (5–16 μm) of hard X-rays with tunable energy achieved via a Si(111) monochromator. Incident energy was typically fixed at 10 keV to excite all target elements simultaneously. Plant tissue (hydrated) was excised from live plants and mounted directly on the sample stage with no further preparation. Samples were rastered in the path of the beam by an XY stage oriented in a plane 45° to the beam, and X-ray fluorescence was detected by a seven-element Canberra Ultra LE-Ge detector (Meriden, CT, USA) positioned 90° to the incident beam. Elemental maps were collected from a 1–3 mm^2 area using a step size of 5 μm (fine map) or 20 μm (coarse map) and a dwell time of 100 ms. In order to isolate the Co signal from contributions of Ni and Fe fluorescence, SXRF images were collected at 50 eV above and below the Co K-edge energy (7.709 keV) and then subtracted to generate a difference map. Sulfur (S) and Co were imaged simultaneously with the incident energy fixed at 1.5 keV above the sulfur K-edge (2472 eV) and the monochromator tuned to pass the third harmonic and fundamental (used to excite the Co K-edge), preventing the Co signal from swamping out the S signal. Additionally, a small helium (He)-purged chamber was attached onto the end of the detector and positioned in tight proximity to the sample to minimize the air path and reduce absorption of the low-energy X-rays.

Microtomography data (DA-CMT and F-CMT) were collected at GeoSoilEnviroCARS (GSECARS) beamline 13-BM-D and 13-ID-C of the Advanced Photon Source at Argonne National Laboratory (Argonne, IL, USA) (Sutton *et al.*, 2002; Rivers & Wang, 2006). Specimens imaged by F-CMT were immersed in liquid nitrogen, freeze-dried under vacuum (–180°C) and mounted on a wooden shaft with epoxy resin, as described by McNear *et al.* (2005). Leaf specimens imaged by DA-CMT were maintained in a high-humidity environment during data collection (approx. 1 h). A leaf was removed from a live plant and immediately placed in a Kapton tube. Dampened cotton was positioned in the tube both above and below the leaf, and the tube was sealed with modeling clay then fixed to a wooden shaft at one end for insertion into the rotation axis of the XYθ stepping stage.

DA-CMT data collection involved exposing the sample to a wide-fan X-ray beam, measuring the transmitted X-rays (converted to visible light via a single-crystal scintillator then projected onto a fast charged-coupled device area detector with a ×10 microscope objective), rotating the sample by a small angle for repeat exposure and continuing the measurements until the sample had been rotated from 0 to 180°. DA-CMT data were collected using 0.25° steps and a 3 s dwell time. Hardware configurations selected for DA-CMT imaging provided optical resolution of 5.12 μm with a 3.27 × 2.59 mm (horizontal × vertical) field of view. Data were acquired with the incident X-ray beam energy set approx. 100 eV below the Co K-edge (7709 eV) or Ni K-edge (8333 eV) energy and then repeated with the beam energy set approx. 30 eV above the absorption edge. Sinograms were reconstructed using the GRIDREC-based software (Dowd *et al.*, 1999). Above- and below-edge data arrays were subtracted and the difference matrices were used to generate the tomographic projections depicting the metal distribution in hydrated leaf tissue.

F-CMT imaging of roots involved a similar procedure, although the samples were rotated and translated in a micro-focused beam (incident energy fixed at 10 keV) and the fluorescence intensities for multiple elements were recorded simultaneously using a 16-element Ge array detector. F-CMT data were collected using 1.5–3° steps, a 1-s dwell time and 5-μm translation steps.

Results

Plant growth

All treatments resulted in healthy looking plants at harvest, and metal treatments did not significantly ($P < 0.05$) affect shoot biomass (Table 1). Cobalt-treated plants (Ni+Co and Ni+Co+Zn) had mild chlorosis on new growth, signifying that the initial Fe concentration in the nutrient solution was inadequate. Plants from the Ni+Co+Zn treatment were less chlorotic than plants exposed to Ni+Co, indicating that the elevated concentration of Zn reduced the antagonism between Co and Fe. Cobalt-induced Fe deficiency was alleviated during the second week of metal exposure by increasing the Fe

Table 1 Shoot biomass and element concentrations for *Alyssum murale* plants 30 d after metal exposure

Ni+Co+Zn treatment (μM)	Shoot biomass	Element concentration in shoot tissue (μg g^{-1} DW)					
	g DW	Ni	Co	Zn	Mn	Fe	S
50-0-0	7.42 a (1.74)	1610 a (189)	–	60.4 a (6.45)	244 a (11.2)	33.3 a (2.61)	5800 a (815)
50-0-50	7.60 a (0.92)	1540 a (302)	–	149 b (42.6)	263 a (31.9)	38.4 a (9.64)	6550 a (978)
50-50-0	6.30 a (0.65)	1650 a (85.1)	1570 a (178)	69.3 a (4.76)	322 b (12.9)	33.5 a (1.40)	8320 b (787)
50-50-50	6.40 a (0.95)	1410 a (139)	2070 b (252)	129 b (20.1)	339 b (29.5)	30.8 a (1.49)	8980 b (730)

Values are mean (± SD); $n = 5$. Different letters within a column indicate significant difference ($P < 0.05$) via Tukey's HSD comparison.

Table 2 Translocation factors (shoot to root concentration ratio) for *Alyssum murale* plants 30 d after metal exposure

Ni+Co+Zn treatment (μM)	Translocation factors					
	Ni	Co	Zn	Mn	Fe	S
50-0-0	1.8 a (0.16)	–	0.09 a (0.01)	0.44 a (0.05)	0.09 a (0.01)	0.53 a (0.07)
50-0-50	2.0 a (0.14)	–	0.07 a (0.01)	0.78 b (0.08)	0.12 a (0.06)	0.58 a (0.06)
50-50-0	1.9 a (0.30)	2.7 a (0.31)	0.12 b (0.02)	0.85 b (0.12)	0.11 a (0.02)	0.80 b (0.07)
50-50-50	2.0 a (0.27)	3.2 a (0.34)	0.07 a (0.01)	1.57 c (0.24)	0.09 a (0.02)	0.86 b (0.08)

Values are mean (± SD); $n = 5$. Different letters within a column indicate significant difference ($P < 0.05$) via Tukey's HSD comparison.

concentration, in all nutrient solutions, to 20 μM. Plants recovered quickly and new growth appeared nonchlorotic. Although the differences in shoot biomass between treatments were insignificant, the slight depression in yield for these Co-treated plants can be attributed to reduced growth during this brief period of mild Fe-deficiency chlorosis.

Bulk characterization of metal accumulation

Elevated aqueous concentrations (50 μM) of Co or Zn in nutrient solution did not significantly ($P < 0.05$) affect the shoot Ni concentration in *A. murale* (Table 1). Plants absorbed Co and Ni to a similar extent from equimolar solutions; root transport systems had comparable ability to shuttle these metals into the vasculature. Zinc was not hyperaccumulated by *A. murale*.

A metal bioconcentration factor (BCF; i.e. the ratio of metal concentration in shoot tissue to metal concentration in growth media) indicates the potential for a plant to concentrate a metal. *A. murale* initially supplied with 50 μM Ni (approx. 3 mg l^{-1} solution) had a shoot Ni concentration averaging 1550 μg g^{-1} dry weight (DW) (BCF approx. 500). In contrast, the maximal Zn BCF was 46 (Ni+Zn). The Co BCFs were 532 (Ni+Co) and 702 (Ni+Co+Zn). Clearly, *A. murale* concentrated Ni and Co against a substantial chemical potential gradient.

A translocation factor (TF; i.e. the ratio of element concentration in shoot tissue to element concentration in root tissue) estimates the translocation efficiency of a plant, and the TF for a hyperaccumulated metal is typically > 1. *A. murale* was efficient at translocating Ni (TF approx. 2) and Co (TF approx. 3), but Zn (TF approx. 0.1) was not translocated to any unusual extent (Table 2). The Ni TF was not significantly altered by elevated concentrations of Co or Zn, indicating minimal effects from the metal co-contaminants. Sulfur and Mn translocation were significantly ($P < 0.05$) affected by the metal treatments, and maximal TFs for S (approx. 0.9) and Mn (approx. 1.6) were observed for plants from the Ni+Co+Zn treatment.

Correlations between the concentration of one metal in shoot tissue and the concentration of other metals or nutrients can help to identify elemental interactions in plants. Cobalt-treated *A. murale* (Ni+Co and Ni+Co+Zn) had significantly ($P < 0.001$) higher shoot concentrations of S and Mn than untreated plants, indicating that the uptake of these elements was related to Co accumulation. *A. murale* had significantly ($P = 0.018$) higher shoot Co concentrations when the Zn concentration was elevated in nutrient solution (Table 1). Maximal shoot Co concentration (2065 μg g^{-1}) and shoot Co accumulation (13.2 mg per plant) were observed for plants from the Ni+Co+Zn treatment.

Plant tissue microanalysis

Metal localization and elemental associations in *A. murale* were investigated with SXRF, CMT, SEM-EDS and XAS. Two-dimensional SXRF images of *A. murale* leaves revealed a distinctive localization pattern for Co relative to Ni and Zn. The Ni distribution in leaves was essentially uniform, although the fluorescence intensity was slightly elevated in the midrib region (Fig. 1). A uniform Ni distribution was anticipated for two-dimensional leaf images because *Alyssum* sequesters Ni within the epidermal layers. The Ni distributions were comparable for both young and old leaves, and Ni localization was not altered in *A. murale* plants exposed to mixed-metal systems (Ni+Co, Ni+Zn, Ni+Co+Zn).

The Zn distribution in *A. murale* leaves appeared similar to that of Ni; however, elevated fluorescence intensity in the midrib region was more evident in SXRF images of Zn than Ni because the Zn fluorescence signal was not dominated by the epidermal cell layers (i.e. more uniform metal distribution through the leaf). Zinc was not hyperaccumulated by *A. murale* and would not be preferentially compartmentalized in epidermal tissue. The Zn distributions were comparable for both young and old leaves.

In contrast to Ni and Zn distributions, Co was preferentially localized at the tips and margins of *A. murale* leaves (Fig. 1). Similar Co localization patterns have been reported for various nonaccumulator plants investigated using autoradiography (^{60}Co radiotracer) (Gustafson, 1956; Langston, 1956; Handreck & Riceman, 1969). Cobalt localization in *A. murale* was consistent for young and old leaves, but Co enrichment near the leaf tips was more common on older leaves than on younger leaves.

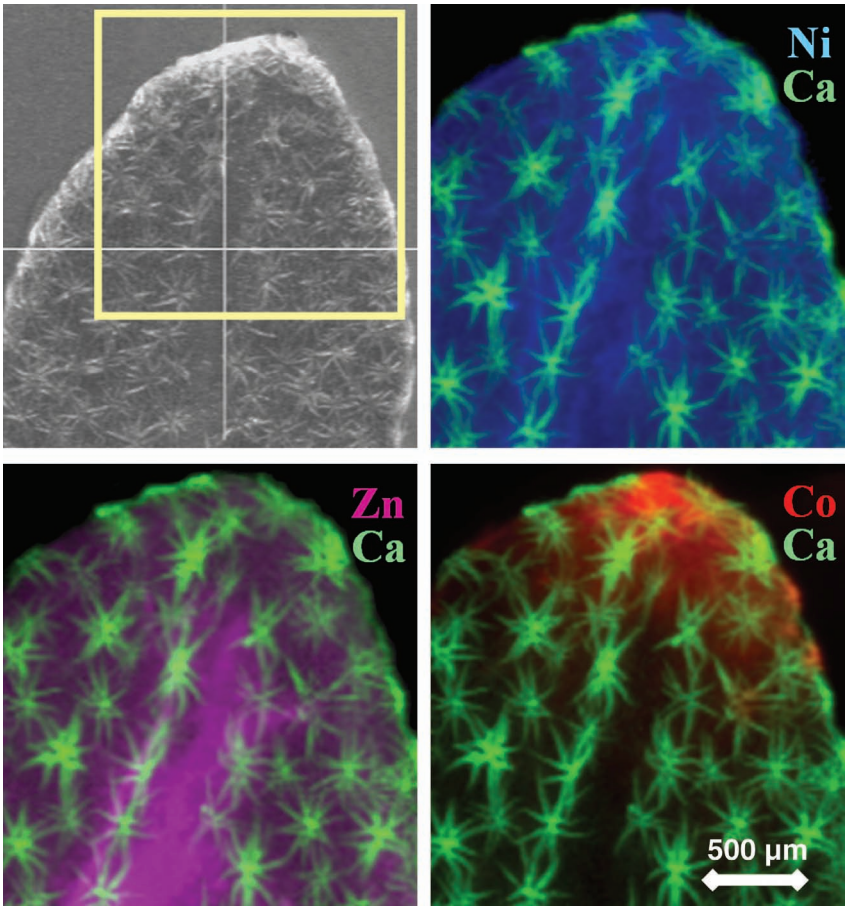

Fig. 1 Synchrotron X-ray microfluorescence (µ-SXRF) images of the nickel (Ni), cobalt (Co), and zinc (Zn) distributions in a hydrated *Alyssum murale* leaf from the Ni+Co+Zn treatment. Leaf trichomes are depicted in the Ca channel. The camera image shows the leaf region selected for SXRF imaging.

Spatial associations in leaves were visualized by combining fluorescence data from individual elements into a multicolor image and plotting a line profile (intensity vs position). An SXRF image of Co, Ni and Ca localization in an *A. murale* leaf revealed a color gradient (blue light plus red light = magenta) near the leaf tip as a result of the uniform Ni distribution and the irregular Co distribution in the leaf (Fig. 2). A line profile generated for a segment from the leaf center towards the leaf tip showed that the substantial increase in the Co signal coincided with a subtle decrease in the Ni signal; Co and Ni were not preferentially co-localized in leaves.

Spatial associations of Co with Mn and S coincided with statistically significant correlations in bulk shoot concentrations. Cobalt-treated plants (Ni+Co and Ni+Co+Zn) had the highest shoot concentrations of Mn and S (Table 1) and the highest S TFs (Table 2). SXRF images of Co and Mn in *A. murale* leaves revealed co-localization of these elements at leaf trichomes (Fig. 3). A Mn-rich zone surrounds the base of *A. murale* trichomes (Fig. 3 inset) and could sequester Ni or Co. SXRF images of S and Co in *A. murale* leaves indicated co-localization of these elements near the leaf tips/margins (Fig. 3). S and Co were spatially correlated, but preliminary XAS data did not indicate a direct chemical association.

Metal localization in *A. murale* roots was investigated with microtomography. F-CMT images of *A. murale* fine-root segments (0.5, 3 and 6 mm from the root apex) revealed distinctive metal partitioning patterns as a function of distance from the root tip (i.e. tissue age and function) (Fig. 4). Nickel, Co and Fe were localized in the root vasculature (procambium) 0.5 mm from the apex; the root tip appeared most active in the absorption of these metals. In the root segment 6 mm from the apex, these metals were predominantly confined to the epidermis, signifying sorption to surface functional groups, mucilage, bacterial biofilms, or metal oxide plaques on the root surface. Additionally, metal enrichment was discernible in the vasculature but was absent from the pith. Similar localization patterns were reported by Fellows *et al.* (2003), who investigated europium (Eu) uptake in living roots of *Avena sativa* and observed maximal fluorescence intensities in the apical tissue at the root tip and within the zone of root maturation (up to 500 µm basipetally), whereas elevated fluorescence from highly differentiated root tissue was observed at the epidermis. Metal localization patterns in the *A. murale* root segment 3 mm from the apex were intermediate to those observed at 0.5 and 6 mm; elevated Ni and Co levels were observed in the vascular cylinder and

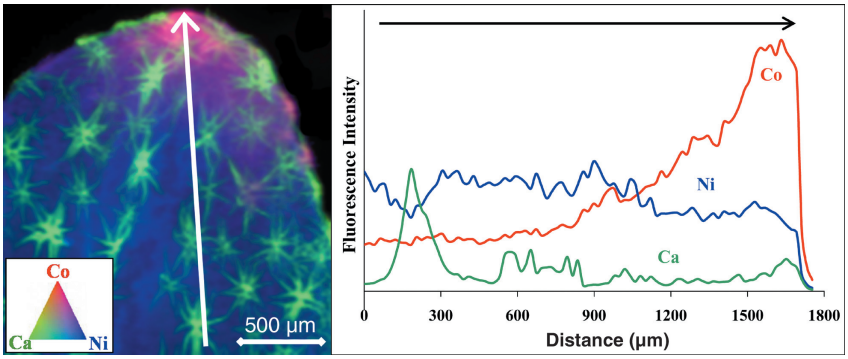

Fig. 2 Synchrotron X-ray microfluorescence (µ-SXRF) tricolor image (nickel (Ni), cobalt (Co), and calcium (Ca)) of a hydrated *Alyssum murale* leaf from the Ni+Co+Zn treatment, plus a line profile (fluorescence intensity vs position) for a segment from the leaf center towards the leaf tip (indicated by a white arrow).

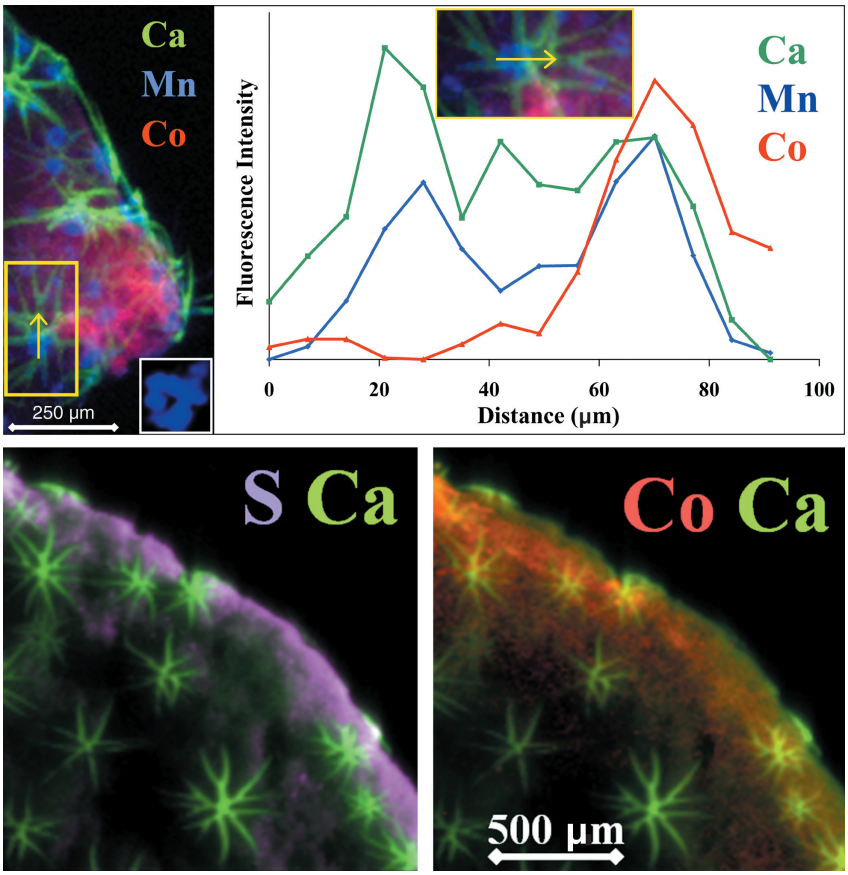

Fig. 3 Synchrotron X-ray microfluorescence (µ-SXRF) images of hydrated *Alyssum murale* leaves from the nickel (Ni) + cobalt (Co) treatment depicting co-localization of Co with (a) manganese (Mn) and calcium (Ca) at a leaf trichome (line profile across the trichome), and (b) sulfur (S) near a leaf tip and margin. The Mn-rich zone (blue) surrounding the trichome base is displayed as an inset on the tricolor SXRF image (top panel).

at the root epidermis. Zinc and Mn localization patterns in *A. murale* roots were distinct from Ni, Co and Fe and from one another (Fig. 4). Zinc was predominantly localized in isolated domains within the root at 0.5, 3 and 6 mm from the apex, whereas Mn was sporadically localized at the epidermis.

A separate experiment conducted with *A. murale* plants exposed to a Co-enriched nutrient solution verified that the Co localization phenomenon observed in the metal interaction study was not a result of simultaneous hyperaccumulation; thus, Co localization had not been altered in plants exposed to elevated Ni and Zn concentrations. Cobalt accumulated by *A. murale* was ultimately deposited on leaf surfaces near the tips/margins. Identical Co localization patterns were observed for Co-treated *A. corsicum* and *A. troodii* (data not shown), suggesting similar mechanisms exist in other Ni hyperaccumulator species of *Alyssum*. Cobalt on the surface of leaves was visible by optical microscopy (Fig. 5 inset). BSE images showed a coating on the leaf surface near the tips/margins, and X-ray microanalysis (SEM-EDS) indicated that the coating was a Co-rich phase (Fig. 5). The electron microprobe beam penetrated only a few microns into

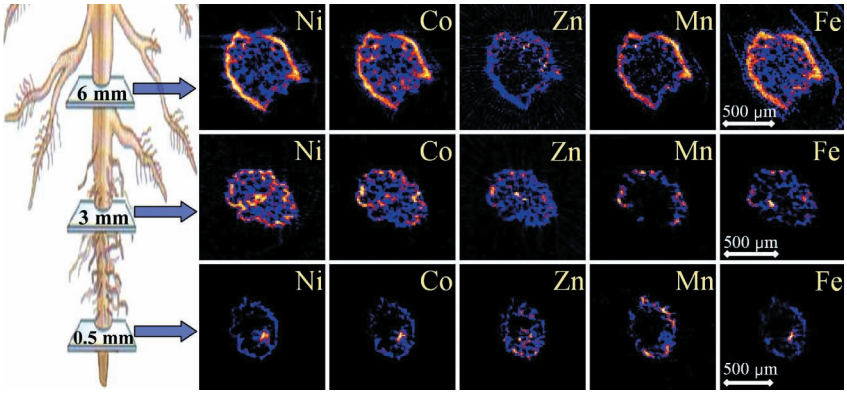

Fig. 4 Fluorescence computed-microtomography (CMT) cross-sectional images (5 µm slices) of the nickel (Ni), cobalt (Co), zinc (Zn), manganese (Mn), and iron (Fe) distributions in *Alyssum murale* fine root segments at 0.5 mm (bottom), 3 mm (middle) and 6 mm (top) from the root apex. Root was collected from the Ni+Co+Zn treatment.

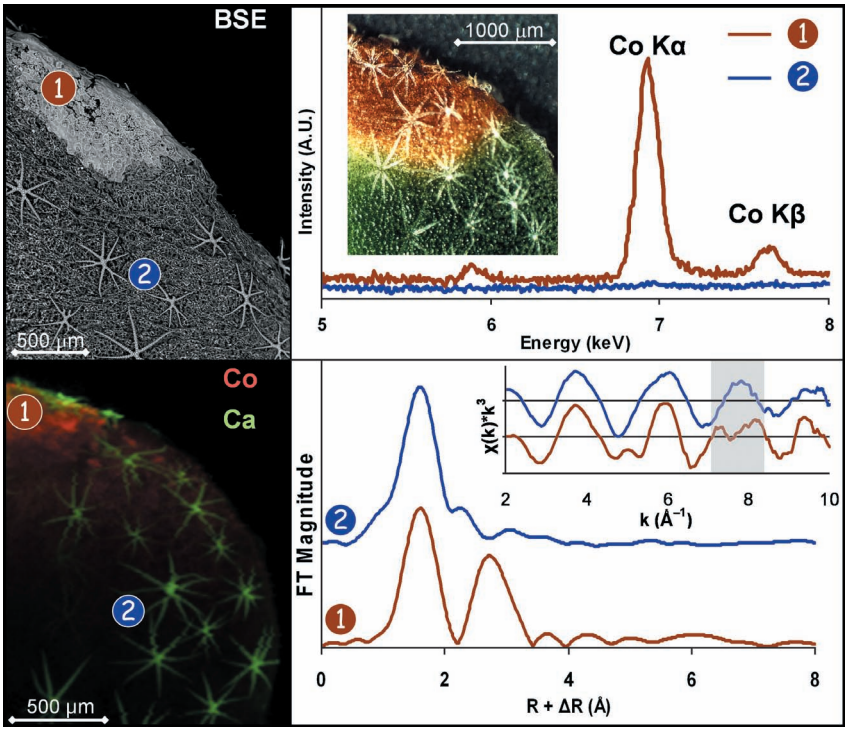

Fig. 5 Backscattered electron (BSE) image of a leaf from cobalt (Co)-treated *Alyssum murale* with the corresponding scanning electron microscopy with energy dispersive X-ray spectroscopy (SEM-EDS) spectra from the leaf-tip and bulk-leaf regions. An optical microscope image of a hydrated leaf from Co-treated *A. murale* is displayed as an inset (top panel); synchrotron X-ray microfluorescence (µ-SXRF) image (Co and calcium (Ca)) of a hydrated leaf from Co-treated *A. murale* with the corresponding Co K-edge k^3-weighted χ (k) spectra (inset) and the Fourier transforms (FT) of µ-XAS spectra from the leaf-tip and bulk-leaf regions (bottom panel).

the sample and thus the recorded signals were emitted from the leaf surface or the cuticle layer; a comparison of EDS spectra from the Co-rich and bulk-leaf regions further supports the finding of a Co-rich phase deposited on the exterior of leaves. Leaf images from the optical microscope and SEM corroborate the Co distribution observed with SXRF (Fig. 5). Micro-XAS spectra collected from hydrated *A. murale* leaves revealed that the oxidation state of Co in plants was Co(II); artificial Co oxidation was not observed in this study, but Co(III) can result from sample alteration in the X-ray beam and by ligand stabilization with multidentate amine ligands (e.g. EDTA). Spectra collected at the Co-rich region near the tip showed striking differences from spectra collected at the bulk-leaf region. The Co k^3-weighted χ(k) spectrum from the Co-rich region had a beat pattern near 5 $Å^{-1}$ and a split oscillation between 7 and 8.5 $Å^{-1}$, whereas the χ(k) spectrum from the bulk-leaf region did not have these characteristic structural features (Fig. 5 inset); spectra with several frequencies (e.g. Co-rich spot 1) are indicative of a long-range ordered binding environment such as that in a mineral structure, whereas spectra dominated by a single frequency (e.g. Bulk-leaf spot 2) are indicative of a short-range ordered environment. An evaluation of the Co-binding environment (*ab initio* model) for Co-rich spot 1 provided distances and numbers of Co–Co pairs that are characteristic of an edge-sharing layered framework. A strong second-shell feature (heavy backscattering

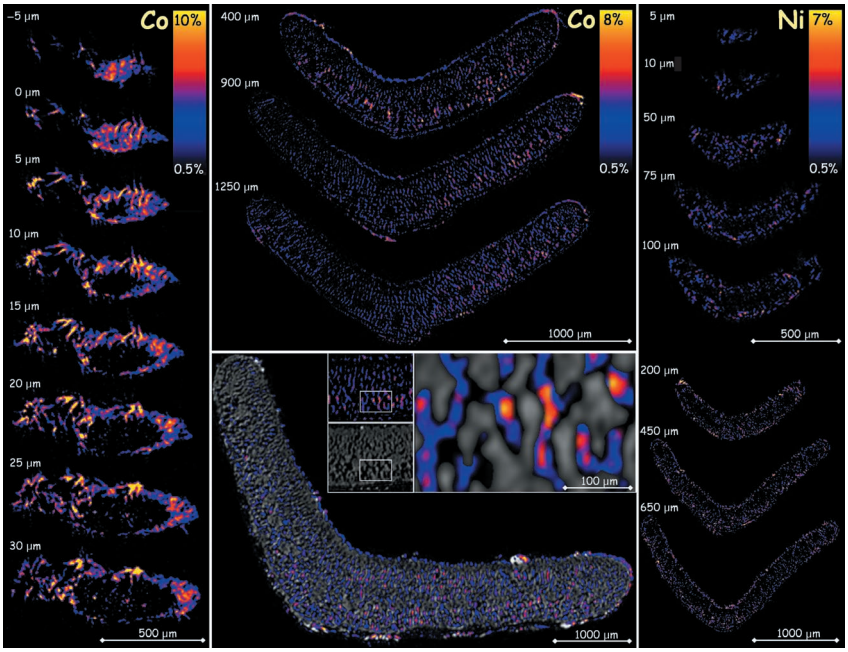

Fig. 6 Differential absorption (DA-CMT) tomographic projections (5.1 µm slices) of hydrated *Alyssum murale* leaves depicting (a) cobalt (Co) distribution in the leaf-tip region, (b) Co distribution in the bulk-leaf region, (c) Co distribution in relation to the leaf cell structure (grey), and (d) nickel (Ni) distribution in the leaf-tip and bulk-leaf regions. Leaves were collected from a Co-treated plant (a–c) and from a Ni-treated plant (d). Sinograms recorded above and below the Co or Ni K-edge energy (+30 eV and –100 eV, respectively) were computationally reconstructed and the resulting projections were subtracted (above – below) to reveal the metal distribution in leaves. Distances are relative to the leaf tissue at the tip as determined from leaf structure images (i.e. below-edge projections).

atom) and a third metal shell at about twice this distance (indicative of a brucite-like hydroxide sheet) was present in the Fourier transform (FT) from the Co-rich region, but was absent in the FT from the bulk-leaf region (Fig. 5). Cobalt accumulated by *A. murale* formed Co-rich mineral precipitate(s) on the leaf surface. Detailed characterization of the Co phase(s) formed on leaves and the ligands involved with Co transport and detoxification in *Alyssum* are beyond the scope of this study but will be reported in a future publication.

DA-CMT images (i.e. virtual cross-sections) of a hydrated leaf from Co-treated *A. murale* revealed a lack of metal enrichment in epidermal tissue (Fig. 6). Cobalt near leaf tips (< 30 µm) was localized predominantly on the leaf exterior. In addition to Co enrichment on the leaf surface, DA-CMT slices 20–30 µm below the leaf tip showed Co localized in isolated regions inside the leaf associated with the vascular system. Cobalt was consistently observed on the exterior of leaves, but deposition on leaf surfaces was less prevalent at greater distances from the leaf tip. Images from several hundreds to thousands of microns below the leaf tip showed a predominance of Co distributed around the leaf ground tissue (intercellular); the distribution between cells was interpreted as Co in the leaf apoplasm (Fig. 6). Cobalt enrichment was more prevalent in the region composed of spongy mesophyll than palisade mesophyll; spongy mesophyll contains fewer chloroplasts and many intercellular spaces linked to the outside via stomata. Regions with elevated Co or Ni were frequently observed in proximity to leaf trichomes; however, Co enrichment was associated with the trichome structures on the leaf surface (i.e. some Co on the leaf surface was trapped in the space between the trichome branches and the leaf tissue), whereas Ni was associated with the basal portion of trichomes. DA-CMT images of a hydrated leaf from Ni-treated *A. murale* showed metal enrichment in the epidermis (Fig. 6); this result is consistent with other studies of Ni compartmentalization in *Alyssum*, which have shown Ni sequestration in epidermal cell vacuoles (Krämer *et al.*, 1997a, 2000; Broadhurst *et al.*, 2004a,b). In addition to epidermal localization, Ni was observed within leaf ground tissue. In contrast to Co, a fraction of Ni in ground tissue occupied the same spaces as mesophyll cells, and this Ni distribution was interpreted as partial metal enrichment of mesophyll tissue.

Discussion

At a fundamental level, mechanisms of metal tolerance and hyperaccumulation in *Alyssum* remain poorly understood. *A. murale* hyperaccumulates Ni and Co, but Zn is not accumulated to abnormal levels. Elevated Co or Zn concentrations (50 µM) do not alter Ni accumulation or localization, and thus *A. murale* can be used to recover Ni from most metal-enriched soils containing these metal co-contaminants. *A. murale* is more tolerant to Ni than Co; nickel (hyper)tolerance is attained via epidermal compartmentalization (i.e. vacuolar sequestration). *A. murale* does not sequester Co in epidermal cells; Co in the xylem or leaf apoplasm is excreted from leaves and subsequently sequestered on leaf surfaces as sparingly soluble precipitate(s). Therefore, the specialized biochemical processes linked to Ni (hyper)tolerance in *A. murale* do not confer (hyper)tolerance to Co.

Metal localization

Cobalt is ultimately deposited at the leaf tips/margins, whereas Ni is sequestered in epidermal cells. Vacuolar sequestration is a key strategy for metal tolerance because leaf epidermal cells provide an effective sink for the accumulated metal. Metal concentrations exceeding 0.35 M were measured in epidermal cell vacuoles of a Zn hyperaccumulator (Küpper *et al.*, 1999). McNear *et al.* (2005) imaged Ni (DA-CMT) in an *A. murale* leaf and reported, in addition to epidermal enrichment, elevated Ni accumulation on/in the leaf tip; furthermore, it was suggested that leaf tips function as an additional reservoir for Ni when concentrations exceed the finite capacity of cell vacuoles. However, McNear *et al.* (2005) did not consider that their leaf tip was curled such that the epidermal layers near the tip were oriented parallel to the incident X-ray beam regardless of the rotation angle; thus, the beam exclusively 'sampled' metal-enriched epidermal tissue in this region, leading to the erroneous impression of elevated Ni on/in the leaf tip (i.e. bright voxels in these upper slices resulted from Ni in the epidermis). Upper slices from the DA-CMT movie (supplementary information, McNear *et al.*, 2005) revealed a lack of Ni enrichment near the point of the leaf (i.e. actual leaf tip); nonetheless, these slices afford a rare glimpse of Ni localization across leaf epidermal tissue.

Clear differences between Ni and Co localization suggest that *A. murale* uses a different metal sequestration mechanism for Co than for Ni. Whereas Ni is redistributed to leaf epidermal cells and subsequently transported across the tonoplast for long-term sequestration in vacuoles (Krämer *et al.*, 1996, 1997a, 2000; Broadhurst *et al.*, 2004a,b), Co does not have an efficient route of entry into epidermal cells. Considering the serpentine (ultramafic) origin of *Alyssum*, a cellular-level tolerance mechanism for Co may not have been naturally selected because the Ni : Co ratio in these soils is relatively large. Additionally, Co is typically retained more strongly by the soil components (e.g. Mn oxides) than Ni and thereby is less phytoavailable (Sparks, 2003). Therefore, mechanisms other than vacuolar sequestration must be operating to cope with the elevated Co concentrations in plant tissue.

A. murale leaves apparently lack the transport system needed to sequester Co in epidermal cells and thus accumulated Co resides in the xylem and the leaf apoplasm. Mass flow and diffusion gradients in the apoplasm will cause Co to redistribute in leaves. Water loss via transpiration will move Co towards the leaf surfaces and margins where transpiration is maximal. Cobalt principally follows the transpiration stream and results in Co enrichment at leaf tips/margins (Kabata-Pendias & Kabata, 1984). When transpiration is low (e.g. at night), root pressure will cause exudation of xylem sap from the ventilation pores (hydathodes) located at the points of the leaf margin to where veins extend (i.e. guttation). Guttation fluids of plants from ultramafic soils have been reported to contain elevated metal (e.g. Mn) concentrations (Mizuno *et al.*, 2002). For example, *Minuartia verna* grown in metal-contaminated soil accumulated Cu and Zn in leaves and excreted these metals onto leaf surfaces via hydathodes (Neumann *et al.*, 1997).

Cobalt accumulated by *A. murale* is ultimately deposited on leaf surfaces. Cobalt enrichment on leaf surfaces is evident from X-ray microtomography (DA-CMT), SEM-EDS, optical microscopy and visual inspection of Co-treated *A. murale* leaves. Similar observations were made by Vergnano & Hunter (1952), who noted red-colored leaf tips on plants exposed to Co-enriched nutrient solution. Cobalt deposition at *A. murale* leaf tips is most prevalent on older leaves. For many plant species, older leaves have the highest concentrations of elements such as Co because evapotranspiration continues as long as the leaf is attached to the plant (Malik *et al.*, 2000). Deposition of sparingly soluble Co species near the tips/margins of *A. murale* leaves is corroborated by *in situ* microspectroscopic analyses (DA-CMT and μ-XAS), revealing that weight percent Co(II) is sequestered on leaf surfaces and forms Co-rich mineral precipitate(s). Metal-tolerant *Arabidopsis halleri* (formerly *Cardaminopsis halleri*), grown in a Zn- and Cu-contaminated soil, had mixed-metal precipitate(s) on leaf surfaces (Neumann & zur Nieden, 2001).

Elevated regions of Ni and Co occur consistently in proximity to the trichomes on *A. murale* leaves, and the Mn-rich zone surrounding the base of trichomes may be partially responsible for this metal enrichment. Simultaneous hyperaccumulation of Mn and Ni occurred in the basal compartment of the nonglandular trichomes on *Alyssum* leaves (Broadhurst *et al.*, 2004b). Metal enrichment of glandular leaf trichomes has been observed in nonaccumulators, such as *Cannabis sativa* with Cu (Arru *et al.*, 2004) and *Nicotiana tabacum* with Zn/Cd (Choi *et al.*, 2001; Sarret *et al.*, 2006). Currently, no consensus exists for the role of Mn in Ni (or Co) sequestration in *Alyssum* or whether the basal compartment of trichomes on hyperaccumulator leaves functions as a significant repository for accumulated metals (Krämer *et al.*, 1997b; Küpper *et al.*, 2000, 2001; Psaras *et al.*, 2000; McNear *et al.*, 2005).

Metal interactions

Shoot Ni concentrations are not appreciably affected for *A. murale* plants cultivated in mixed-metal systems containing less than 50 μM Co or Zn. Plants from the Ni+Co+Zn treatment have the highest shoot Co concentrations, suggesting that Zn has a synergistic effect on Co uptake; the effects of Co on plants was reviewed by Palit *et al.* (1994) who noted that Zn often interacts synergistically with Co. Cobalt-treated *A. murale* (Ni+Co and Ni+Co+Zn) had significantly higher shoot S and Mn concentrations than untreated plants. Enhanced S uptake by plants, and elevated S in Co-rich leaf regions, may be related to a charge balance requirement. Other researchers have found highly significant correlations between S and Ni in individual cells of *Alyssum* using

SEM-EDS and attributed the co-localization to SO_4^{2-} functioning as a counter ion (Küpper *et al.*, 2001; Broadhurst *et al.*, 2004a). Enhanced Mn uptake by *A. murale* plants from the Ni+Co and Ni+Co+Zn treatments may be related to the stability of transition metal complexes; the Irving-Williams series (Irving & Williams, 1948) predicts displacement of Mn from anionic functional groups (e.g. xylem cell wall surfaces) in the presence of Ni, Co, or Zn.

Competition between metals is not evident under the conditions imposed in this study. Cobalt frequently interacts antagonistically with Ni, Fe and Mn in plants (Kabata-Pendias & Kabata, 1984; Palit *et al.*, 1994), and antagonistic interactions between Ni and Co are observed for *Alyssum* species under specific experimental conditions. For instance, Gabbrielli *et al.* (1991) evaluated Co and Zn tolerance and uptake in the Ni hyperaccumulator, *Alyssum bertolonii*, and suggested that plants were tolerant to Co and Zn but noted that these metals compete with Ni accumulation; this antagonistic interaction occurred with *Alyssum* seedlings during a toxicity assay (i.e. very high metal concentrations). *Alyssum* plants hyperaccumulated Co (1320 mg kg^{-1} DW) from a Co-amended soil but accumulated significantly less Co (< 20 mg kg^{-1} DW) from a refinery-contaminated soil with a high Ni to Co ratio (70 : 1) (Malik *et al.*, 2000). Cobalt and Ni accumulation by *Alyssum* species in single and mixed-metal media (several hundred mg kg^{-1} metal) was investigated by Homer *et al.* (1991), who attributed lower Ni levels in plants to suppressed Ni uptake by Co ions.

Nickel and Co are expected to interact antagonistically as a result of competition for semiselective transport proteins in roots, whereas Zn is not expected to interfere appreciably with Ni absorption (except by cation competition) because it is not hyperaccumulated by *Alyssum*. High Ni and Co concentrations will increase competition for root metal transporters and for intercellular ligands participating in metal absorption, long-distance transport, or metal detoxification. Exposure of the hyperaccumulator, *Alyssum lesbiacum*, to Ni resulted in a dose-dependent increase in xylem sap Ni concentration and total histidine (Krämer *et al.*, 1996); thermodynamic calculations (Geochem PC) predicted that nearly all histidine (> 97%) was complexed with Ni. Kerkeb & Krämer (2003) later suggested a role for histidine in radial transport and xylem loading of Ni in *Alyssum*. Nickel/Co antagonism in *Alyssum* may be related to competition for intercellular ligands. Ligands with a greater affinity for Ni than for Co can facilitate selective accumulation (Still & Williams, 1980); however, selective accumulation or antagonistic interactions may not be evident unless the free metal ion (Ni+Co) concentration exceeds the concentration of metal-binding ligands.

Metal tolerance and sequestration

Metal tolerance and accumulation mechanisms in *A. murale* do not appear to be directly correlated. *A. murale* concentrates Ni in shoot tissue to abnormal levels (hyperaccumulation mechanism) and has a Ni-specific tolerance mechanism (vacuolar sequestration) to prevent damage to photosynthetically active tissue. Similarly, *A. murale* concentrates Co in shoot tissue but lacks an equivalent cellular-level sequestration mechanism to confer Co tolerance. In fact, Morrison (1980) noted that *Alyssum* is less tolerant to Co than to Ni. An underlying relationship between metal accumulation and tolerance remains unclear. For instance, variability in Zn tolerance between populations of *Thlaspi caerulescens* from a contaminated Zn mine and an uncontaminated site was not associated with a variation in the ability to accumulate Zn, suggesting that tolerance and hyperaccumulation were independent traits (Ingrouille & Smirnoff, 1986). Similarly, high metal transport ability was coupled with low metal tolerance in the nonaccumulator *Thlaspi arvense* (Krämer *et al.*, 1997a). While correlations between hyperaccumulation and tolerance have been observed in populations of taxonomically related hyperaccumulator and nonaccumulator species (Homer *et al.*, 1991; Krämer *et al.*, 1996, 1997a; Chaney *et al.*, 1997; Salt & Krämer, 2000), intraspecies comparisons have revealed independent genetic variation in these two traits for *T. caerulescens* (Macnair *et al.*, 1999, 2000; Schat *et al.*, 2000; Pollard *et al.*, 2002; Frérot *et al.*, 2005) and *A. halleri* (Macnair *et al.*, 1999; Bert *et al.*, 2003).

Tolerance strategies are typically metal specific (Schat *et al.*, 2000; Walker & Bernal, 2004), relying on unique biochemical processes to mediate metal transport across cell membranes (e.g. vacuolar tonoplast) as well as intercellular ligands for chelation of metals (Schat *et al.*, 2000). Previous research has identified the importance of organic and amino acids in metal transport and detoxification in hyperaccumulators (e.g. *Alyssum* and *Thlaspi*). As free metal ions are the most cytotoxic form of trace elements (e.g. Co and Ni), accumulator plants need specialized tolerance mechanisms to prevent disruption of normal metabolic functions. Accumulator plants attain (hyper)tolerance through chemical binding (detoxification) and intracellular sequestration (Brooks *et al.*, 1977; Baker, 1981; Küpper & Kroneck, 2005).

A. murale plants alleviate Co toxicity via an exocellular sequestration mechanism. Depending on the definition of tolerance, one can argue that *A. murale* achieves Co tolerance through a chemical-binding mechanism, presumably involving O and N donor ligands, coupled to an exclusion mechanism involving excretion (possibly via hydathodes) and deposition of the metal on leaf surfaces. Deposition on leaf surfaces exposes the metal species to diverse environmental conditions (e.g. microbial activity, dehydration, light, etc.) and can lead to the formation of sparingly-soluble phases via molecular-level restructuring. Cobalt excreted from *A. murale* forms Co-rich mineral precipitate(s) on leaf surfaces. Several component mechanisms of metal tolerance can be recognized: (1) metal detoxification via complexation with ligands; (2) metal sequestration in cellular compartments; (3) metal

sequestration via exocellular deposition; and (4) metal detoxification by formation of sparingly-soluble phases.

Ultimately, understanding the physiological and biochemical processes underlying metal acquisition, accumulation and tolerance will permit optimization of metal phytoextraction and aid developments in the production of nutrient-fortified foods. A mechanistic understanding of the highly selective metal transport system linked to Ni tolerance in *A. murale* (vacuolar transporter of leaf epidermal cells) should prove useful for identifying metal transporter(s) in roots or xylem, thus offering insight to the lack of metal selectivity at the plant–mineral–H_2O interface. Accumulator plants with the capacity for 'simultaneous hyperaccumulation' can evolve with a cellular-level tolerance mechanism for one metal (Ni) but may not develop a similar mechanism to confer (hyper) tolerance for a co-accumulated metal (Co), especially when environmental conditions limit the need for adaptation (e.g. low bioavailability in the natural environment). These data agree with previous hypotheses and support observations suggesting that metal tolerance and accumulation mechanisms can be independent. Accumulator plants lacking cellular-level tolerance for an accumulated metal must resort to alternate sequestration strategies to maintain metal homeostasis; *A. murale* relies on an exocellular sequestration mechanism for Co. *A. murale* can be used to remediate Co-enriched soils or industrial wastewater in select circumstances, and Ni phytomining can occur successfully with elevated Co or Zn in (soil) solution.

Acknowledgements

Special thanks are extended to Jennifer Ciconte (Phytosystems) and Rodney Dempsey (Fischer Greenhouse, UD) for maintenance of plant cultivation systems, and to Jen Seiter (Environmental Soil Chemistry, UD) and Sirine Fakra (Advanced Light Source, LBNL) for assistance with microspectroscopic experiments. The operations of the Advanced Light Source at Lawrence Berkeley National Laboratory were supported by the Director, Office of Science, Office of Basic Energy Sciences, US Department of Energy under Contract no. DE-AC02–05CH11231. Portions of this work were performed at GeoSoilEnviroCARS (Sector 13), Advanced Photon Source (APS), Argonne National Laboratory. We greatly appreciate the assistance from Drs Steve Sutton and Matt Newville with F-CMT experiments. GeoSoilEnviroCARS is supported by the National Science Foundation – Earth Sciences (EAR-0217473), Department of Energy – Geosciences (DE-FG02–94ER14466) and the State of Illinois. Use of the APS was supported by the US Department of Energy, Basic Energy Sciences, Office of Energy Research, under Contract No. W-31–109-Eng-38. We are grateful to Kristian Paul, Carole Gross, Noelle Gameros and several anonymous reviewers for their suggestions to improve the manuscript. Ryan Tappero appreciates support from a USDA Graduate Research Fellowship and a University of Delaware Academic Fellowship.

References

Adriano DC. 1986. *Trace elements in the terrestrial environment.* New York, NY, USA: Springer-Verlag, Inc., 1–18.

Arru L, Rognoni S, Baroncini M, Bonatti PM, Perata P. 2004. Copper localization in *Cannabis sativa* L. grown in a copper-rich solution. *Euphytica* **140**: 33–38.

Baker AJM. 1981. Accumulators and excluders – strategies in the response of plants to heavy metals. *Journal of Plant Nutrition* **3**: 643–654.

Bert V, Meerts P, Saumitou-Laprade P, Salis P, Gruber W, Verbruggen N. 2003. Genetic basis of Cd tolerance and hyperaccumulation in *Arabidopsis halleri. Plant Soil* **249**: 9–18.

Bidwell SD, Crawford SA, Woodrow IE, Sommer-Knudsen J, Marshall AT. 2004. Sub-cellular localization of Ni in the hyperaccumulator *Hybanthus floribundus* (Lindley) F. Muell. *Plant, Cell & Environment* **27**: 705–716.

Broadhurst CL, Chaney RL, Angle JA, Erbe EF, Maugel TK. 2004a. Nickel localization and response to increasing Ni soil levels in leaves of the Ni hyperaccumulator *Alyssum murale. Plant Soil* **265**: 225–242.

Broadhurst CL, Chaney RL, Angle JS, Maugel TK, Erbe EF, Murphy CA. 2004b. Simultaneous hyperaccumulation of nickel, manganese, and calcium in *Alyssum* leaf trichomes. *Environmental Science & Technology* **38**: 5797–5802.

Brooks RR, Lee J, Reeves RD, Jaffre T. 1977. Detection of nickeliferous rocks by analysis of herbarium specimens of indicator plants. *Journal of Geochemistry and Exploration* **7**: 49–57.

Chaney RL. 1983. Plant uptake of inorganic waste constituents. In: Parr JF, Marsh PB, Kla JM, eds. *Land treatment of hazardous wastes.* Park Ridge, NJ, USA: Noyes Data Corp., 50–76.

Chaney RL. 1988. Plants can utilize iron from Fe-N,N′-di-(2-hydroxybenzoyl)-ethylenediamine-N,N′-diacetic acid, a ferric chelate with 10^6 greater formation constant than Fe-EDDHA. *Journal of Plant Nutrition* **11**: 1033–1050.

Chaney RL, Malik M, Li YM, Brown SL, Brewer EP, Angle JS, Baker AJM. 1997. Phytoremediation of soil metals. *Current Opinions in Biotechnology* **8**: 279–284.

Chaney RL, Angle JS, Baker AJM, Li YM. 2004. *Method for phytomining of nickel, cobalt, and other metals from soil.* US patent 5,944,872.

Choi YE, Harada E, Wada M, Tsuboi H, Morita Y, Kusano T, Sano H. 2001. Detoxification of cadmium in tobacco plants: formation and active excretion of crystals containing cadmium and calcium through trichomes. *Planta* **213**: 45–50.

Dixon NE, Gazola C, Blakeley RL, Zerner B. 1975. Jack bean urease (EC 3.5.1.5), a metalloenzyme. A simple biological role for nickel? *Journal of the American Chemistry Society* **97**: 4131–4133.

Dowd BA, Campbell GH, Marr RB, Nagarkar VV, Tipnis SV, Axe L, Siddons DP. 1999. Developments in synchrotron X-ray computed microtomography at the National Synchrotron Light Source. *Proceedings of SPIE, Developments in X-Ray Tomography II* **3772**: 224–236.

Fellows RJ, Wang Z, Ainsworth CC. 2003. Europium uptake and partitioning in Oat (*Avena sativa*) roots as studied by laser-induced fluorescence spectroscopy and confocal microscopy profiling technique. *Environmental Science & Technology* **37**: 5247–5253.

Frérot H, Lefèbvre C, Petit C, Collin C, Dos Santos A, Escarré J. 2005. Zinc tolerance and hyperaccumulation in F1 and F2 offspring from intra and interecotype crosses of *Thlaspi caerulescens. New Phytologist* **165**: 111–119.

Frey B, Keller C, Zierold K, Schulin R. 2000. Distribution of Zn in functionally different leaf epidermal cells of the hyperaccumulator *Thlaspi caerulescens. Plant, Cell & Environment* **23**: 675–687.

Gabbrielli R, Mattioni C, Vergnano O. 1991. Accumulation mechanisms and heavy metal tolerance of a nickel hyperaccumulator. *Journal of Plant Nutrition* **14**: 1067–1080.

Gustafson FG. 1956. Absorption of ^{60}Co by leaves of young plants and its translocation through the plant. *American Journal of Botany* **43**: 157–160.

Hamilton EI. 1994. The geobiochemistry of cobalt. *Science of the Total Environment* **150**: 7–39.

Handreck KA, Riceman DS. 1969. Cobalt distribution in several plant species grown in culture solutions. *Australian Journal of Agricultural Research* **20**: 213–226.

Heath SM, Southworth D, Allura JAD. 1997. Localization of nickel in epidermal subsidiary cells of leaves of *Thlaspi montanum var. siskiyouense* (Brassicaceae) using energy-dispersive X-ray microanalysis. *International Journal of Plant Science* **158**: 184–188.

Homer FA, Morrison RS, Brooks RR, Clemens J, Reeves RD. 1991. Comparative studies of nickel, cobalt, and copper uptake by some nickel hyperaccumulators of the genus *Alyssum*. *Plant Soil* **138**: 195–205.

Ingrouille MJ, Smirnoff N. 1986. *Thlaspi caerulescens* J. & C. Presl. (*T. alpestre* L.) in Britain. *New Phytologist* **102**: 219–233.

Irving H, Williams RJP. 1948. Order of stability of metal complexes. *Nature* **6**: 746–747.

Kabata-Pendias A, Kabata H. 1984. Elements of Group VIII. In: *Trace elements in soils and plants*. Boca Raton, FL, USA: CRC Press Inc., 238–246.

Kerkeb L, Krämer U. 2003. The role of free histidine in xylem loading of nickel in *Alyssum lesbiacum* and *Brassica juncea*. *Plant Physiology* **131**: 716–724.

Kim SA, Punshon T, Lanzirotti A, Li L, Alonso JM, Ecker JR, Kaplan J, Guerinot ML. 2006. Localization of iron in *Arabidopsis* seed requires the vacuolar membrane transporter VIT1. *Science* **314**: 1295–1298.

Krämer U, Cotterhowells JD, Charnock JM, Baker AJM, Smith JC. 1996. Free histidine as a metal chelator in plants that accumulate nickel. *Nature* **379**: 635–638.

Krämer U, Smith RD, Wenzel WW, Raskin I, Salt DE. 1997a. The role of metal transport and tolerance in nickel hyperaccumulation by *Thlaspi goesingense* Halacsy. *Plant Physiology* **115**: 1641–1650.

Krämer U, Grime GW, Smith JAC, Hawes CR, Baker AJM. 1997b. Micro-PIXE as a technique to study nickel localization in leaves of the hyperaccumulator plant *Alyssum lesbiacum*. *Nuclear Instruments and Methods in Physics Research B* **130**: 346–350.

Krämer U, Pickering IJ, Prince RC, Raskin I, Salt DE. 2000. Subcellular localization and speciation of nickel in hyperaccumulator and non-accumulator *Thlaspi* species. *Plant Physiology* **122**: 1343–1354.

Kukier U, Peters CA, Chaney RL, Angle JS, Roseberg RJ. 2004. The effect of pH on metal accumulation in two *Alyssum* species. *Journal of Environmental Quality* **33**: 2090–2102.

Küpper H, Zhao FJ, McGrath SP. 1999. Cellular compartmentation of zinc in leaves of the hyperaccumulator *Thlaspi caerulescens*. *Plant Physiology* **119**: 305–311.

Küpper H, Lombi E, Zhao FJ, McGrath SP. 2000. Cellular compartmentation of cadmium and zinc in relation to other elements in the hyperaccumulator *Arabidopsis halleri*. *Planta* **212**: 75–84.

Küpper H, Lombi E, Zhao FJ, Wieshammer G, McGrath SP. 2001. Cellular compartmentation of nickel in the hyperaccumulator *Alyssum lesbiacum*, *Alyssum bertolonii*, and *Thlaspi goesingense*. *Journal of Experimental Botany* **52**: 2291–2300.

Küpper H, Kroneck PMH. 2005. Heavy metal uptake by plants and cyanobacteria. In: Sigel A, Sigel H, Sigel Royal, eds. *Metal ions in biological systems*, Vol. 44. New York, NY, USA: Marcel Dekker, 97–142.

Langston R. 1956. Distribution patterns of radioisotopes in plants. *Proceedings of the American Society of Horticultural Science* **68**: 370–376.

Li YM, Chaney RL, Brewer E, Roseberg R, Angle JS, Baker AJM, Reeves R, Nelkin J. 2003a. Development of a technology for commercial phytoextraction of nickel: economic and technological considerations. *Plant Soil* **249**: 107–115.

Li YM, Chaney RL, Brewer EP, Angle JS, Nelkin J. 2003b. Phytoextraction of nickel and cobalt by hyperaccumulator *Alyssum* species grown on nickel-contaminated soils. *Environmental Science & Technology* **37**: 1463–1468.

Macnair MR, Bert V, Huitson SB, Saumitou-Laprade P, Petit D. 1999. Zinc tolerance and hyperaccumulation are genetically independent characters. *Proceedings of the Royal Society of London B* **266**: 2175–2179.

Macnair MR, Tilstone GH, Smith SE. 2000. The genetics of metal tolerance and accumulation in higher plants. In: Terry N, Bañuelos G, eds. *Phytoremediation of contaminated soil and water*. Boca Raton, FL, USA: Lewis Publishers, 235–250.

Malik M, Chaney RL, Brewer EP, Li Y, Angle JS. 2000. Phytoextraction of soil cobalt using hyperaccumulator plants. *International Journal of Phytoremediation* **2**: 319–329.

Marcus MA, MacDowell AA, Celestre R, Manceau A, Miller T, Padmore HA, Sublett RE. 2004. Beamline 10.3.2 at ALS: a hard X-ray microprobe for environmental and materials sciences. *Journal of Synchrotron Radiation* **11**: 239–247.

Marschner H. 1995. *Mineral nutrition of higher plants*, 2nd edn. New York, NY, USA: Academic Press.

McNear DH Jr, Peltier E, Everhart J, Chaney RL, Newville M, Rivers M, Sutton S, Sparks DL. 2005. Application of quantitative fluorescence and absorption-edge computed microtomography to image metal compartmentalization in *Alyssum murale*. *Environmental Science and Technology* **39**: 2210–2218.

Mesjasz-Przybylowicz J, Przybylowicz WJ, Prozesky VW, Pineda CA. 1997. Quantitative micro-PIXE comparison of elemental distribution in Ni-hyperaccumulating and non-accumulating genotypes of *Senecio coronatus*. *Nuclear Instruments and Methods in Physics Research B* **130**: 368–373.

Mizuno N, Takahashi A, Wagatsuma T, Mizuno T, Obata H. 2002. Chemical composition of guttation fluid and leaves of *Petasites japonicus* var. giganteus and *Polygonum cuspidatum* growing on ultramafic soil. *Soil Science Plant Nutrition* **48**: 451–453.

Morrison Richard S. 1980. *Aspects of the accumulation of cobalt, copper, and nickel by plants*. PhD Thesis, Massey University, Palmerton North, New Zealand.

Neumann D, zur Nieden U. 2001. Silicon and heavy metal tolerance of higher plants. *Phytochemistry* **56**: 685–692.

Neumann D, zur Nieden U, Schwieger W, Leopold I, Lichtenberger O. 1997. Heavy metal tolerance of *Minuartia verna*. *Journal of Plant Physiology* **151**: 101–108.

Norkus E, Vaskelis A, Griguceviciene A, Rozovskis G, Reklaitis J, Norkus P. 2001. Oxidation of cobalt (II) with air oxygen in aqueous ethylenediamine solutions. *Transition Metal Chemistry* **26**: 465–472.

Palit S, Sharma A, Talukder G. 1994. Effects of cobalt on plants. *Botany Reviews* **60**: 149–181.

Pollard AJ, Powell KD, Harper FA, Smith JAC. 2002. The genetic basis of metal hyperaccumulation in plants. *Critical Reviews in Plant Science* **21**: 539–566.

Psaras GK, Constantinidis T, Cotsopoulos B, Manetas Y. 2000. Relative abundance of nickel in the leaf epidermis of eight hyperaccumulators: evidence that the metal is excluded from both guard cells and trichomes. *Annals of Botany* **86**: 73–78.

Rivers M, Wang Y. 2006. Recent developments in microtomography at GeoSoil-EnviroCARS. *Proceedings of SPIE, Developments in X-ray tomography*. **V. 631**(0J-): 1–15.

Salt DE, Krämer U. 2000. Mechanism of metal hyperaccumulation in plants. In: Raskin L, Ensley BD, eds. *Phytoremediation of toxic metals*. New York, NY, USA: John Wiley, 231–236.

Sarret G, Harada E, Choi YE, Isaure MP, Geoffroy N, Birschwilks M, Clemens S, Fakra S, Marcus MA, Manceau A. 2006. Trichomes of tobacco excrete zinc as Zn-substituted calcium carbonate and other Zn-containing compounds. *Plant Physiology* **141**: 1021–1034.

Schat H, Llugany M, Bernhard R. 2000. Metal-specific patterns of tolerance, uptake, and transport of heavy metals in hyperaccumulating and nonhyperaccumulating metallophytes. In: Terry N, Bañuelos G, eds. *Phytoremediation of contaminated soil and water*. Boca Raton, FL, USA: Lewis Publishers, 171–188.

Scheckel KG, Lombi E, Rock SA, McLaughlin MJ. 2004. *In vivo* synchrotron study of Thallium speciation and compartmentalization in *Iberris intermedia. Environmental Science Technology* **38**: 5095–5100.

Sparks DL. 2003. *Environmental Soil Chemistry*, 2nd edn. New York, NY, USA: Academic Press, 133–186.

Still ER, Williams RJP. 1980. Potential methods for selective accumulation of Nickel (II) ions by plants. *Journal of Inorganic Biochemistry* **13**: 35–40.

Sutton S, Bertsch PM, Newville M, Rivers M, Lanzirotti A, Eng P. 2002. Microfluorescence and microtomography analyses of heterogeneous earth and environmental materials. In: Fenter PM, Rivers M, Sturchio N, Sutton S, eds. *Applications of synchrotron radiation in low-temperature geochemistry and environmental science*, Vol. 49. Washington DC, USA: Mineralogical Society of America, 429–483.

Vergnano O, Hunter JG. 1952. Nickel and cobalt toxicities in Oat plants. *Annals of Botany* **17**: 317–329.

Walker DJ, Bernal MP. 2004. The effects of copper and lead on growth and zinc accumulation of *Thlaspi caerulescens* J. & C. Presl: implications for phytoremediation of contaminated soils. *Water Air Soil Pollution* **151**: 361–372.

Welch RM. 1995. Micronutrient nutrition of plants. *Critical Reviews in Plant Science* **14**: 49–82.